

Impact of oxygen vacancies in Ni supported mixed oxide catalysts on anisole hydrodeoxygenation

Hadi Ali^{a,b}, Tom Vandevyvere^{b,c}, Jeroen Lauwaert^c, Sushil Kumar Kansal^d,
Shunmugavel Saravanamurugan^{a,*}, Joris W. Thybaut^{b,*}

^a Laboratory of bioproduct Chemistry, Center of Innovative and Applied Bioprocessing, Sector 81 (Knowledge City), Mohali 140306, Punjab, India

^b Laboratory for Chemical Technology (LCT), Ghent University, Technologiepark 125, 9052 Ghent, Belgium

^c Industrial Catalysis and Adsorption Technology (INCAT), Valentin Vaerwyckweg 1, 9000 Ghent, Belgium

^d Department of Chemical Engineering and Technology, Panjab University, Chandigarh 160014, India

ARTICLE INFO

Keywords:

Hydrodeoxygenation
Anisole
Benzene
Oxophilic sites
Oxygen vacancy sites
Nickel
Zirconium oxide

ABSTRACT

The hydrodeoxygenation (HDO) activity of anisole has been investigated over Ni catalysts on mixed metal oxide supports containing Nb–Zr and Ti–Zr in 1:1 and 1:4 ratios. XRD patterns indicate the incorporation of Ti (or Nb) into the ZrO₂ framework. XPS and oxygen pulse chemisorption analyses reveal that Ni/Ti₁Zr₄ and Ni/Nb₁Zr₄ possessed more oxygen vacancy sites than Ni/Ti₁Zr₁ and Ni/Nb₁Zr₁, respectively. Correspondingly, the HDO activity of Ni/Ti₁Zr₄ and Ni/Nb₁Zr₄ was higher with an anisole conversion up to 30.7 and 34.4%, with high selectivity towards benzene (up to 64.7 and 63.3%), compared to corresponding Ni/Ti₁Zr₁ and Ni/Nb₁Zr₁ catalysts.

1. Introduction

The surplus availability of terrestrial lignocellulosic biomass (LCB) signifies its potential as an alternative to fossil fuels for fulfilling growing energy demands [1]. Among the significant fractions of LCB, lignin is an intricate aromatic heteropolymer with high C/O content. Currently, lignin produced from the pulp and paper industry remains underutilized as a low-value fuel source [2]. The pyrolysis of lignin to bio-oil is a promising approach and exhibits a good fuel source. However, the high oxygen content in the form of -OCH₃ and -OH groups provokes corrosive behavior and reduces storage stability, thus limiting the potential of oil transportation [3]. To overcome these issues, hydrodeoxygenation (HDO) can be employed as a process that can efficiently reduce the oxygen content in aromatic compounds [4].

Several articles have reported the HDO of lignin model compounds, such as phenol, anisole and guaiacol, over a wide range of supported metal-containing catalysts to produce corresponding deoxygenated product(s) with high selectivity [5]. Among the investigated catalysts for HDO, Ni-based ones have received quite some attention due to their cost-effectiveness, easy availability and comparable catalytic activity to noble metals [6]. Monometallic Ni on an inert support, such as SiO₂, has been proven to be active for phenol and m-cresol conversion exhibiting

mainly a selectivity towards hydrogenation products (cyclohexanol/cyclohexanone) rather than to deoxygenation products (benzene/toluene) [7]. Auxiliary active metal(s) on suitable support(s) are, hence, required to enhance the deoxygenation activity, preferably at the expense of the hydrogenation activity. To improve the HDO performance, oxophilic metals, such as Fe and Ga have been incorporated into Ni/SiO₂ [8,9], as they can increase the interaction between oxophilic sites and the oxygen moiety of the oxygenated compounds. The introduction of an auxiliary metal reduced the Ni particle size, thus increasing the electron density around the Ni particles by forming alloy and intermetallic compounds, enhancing the activity [9].

Not only the active metal(s), but also the monoxide support can play a crucial role in improving the deoxygenation activity. Yang et al. found that Ni/TiO₂ gave the highest benzene selectivity (80%) with 50% anisole conversion among the tested catalysts (CeO₂, γ-Al₂O₃, SBA-15 and carbon) due to strong metal-support interaction [10]. Further, Ru/NbO improved the oxygen vacancy upon incorporating Fe due to its oxophilic character, thus indicating the importance of suitable auxiliary metal oxide [11]. Likewise, a similar trend has been observed for RuFe/TiO₂ [12]. Moreover, the superior performance observed over mixed metal oxide supports was attributed to a high surface area and improved oxygen vacancy site availability [13,14]. 10 wt%Ni supported on

* Corresponding authors.

E-mail addresses: saravana@ciab.res.in (S. Saravanamurugan), joris.thybaut@ugent.be (J.W. Thybaut).

<https://doi.org/10.1016/j.catcom.2022.106436>

Received 17 December 2021; Received in revised form 2 February 2022; Accepted 21 February 2022

Available online 23 February 2022

1566-7367/© 2022 The Author(s).

Published by Elsevier B.V. This is an open access article under the CC BY-NC-ND license

(<http://creativecommons.org/licenses/by-nc-nd/4.0/>).

Ce_{0.3}Nb_{0.7} exhibited an excellent benzene selectivity (87%) compared to Ni/CeO₂ (8%) and decreased the formation of hydrogenation products, indicating the crucial role of Nb on deoxygenated products [14]. The rationale behind the improved activity was correlated to the formation of enhanced oxygen vacancy sites, facilitating the activation of C_{Ar}-O of phenol to yield the deoxygenated product benzene. Despite the promising performance, the area of HDO of phenolic compounds with Ni supported mixed oxide catalysts remained largely unexplored [13,14].

The catalytic materials developed so far present significant challenges, such as a large amount of Ni that was employed, the selectivity towards hydrogenation products and inadequate oxophilic sites. Hence, the current work reports the synthesis of Ni-doped (typically 3 wt%) mixed metal oxide supports by incorporating Ti or Nb into the ZrO₂ network to enhance oxygen vacancy site formation and their catalytic activity towards anisole HDO in a continuous-flow reactor. The oxygen vacancy sites of the Ni/NbZr and Ni/TiZr catalysts are examined using techniques such as XPS, O₂-pulse chemisorption and XRD and discussed accordingly.

2. Experimental

2.1. Catalyst preparation and catalytic testing

The synthesis procedure of 3 wt% Ni loaded on mixed oxide supports (Ni/Ti₁Zr₁, Ni/Ti₁Zr₄, Ni/Nb₁Zr₁ and Ni/Nb₁Zr₄) is given in ESI. The catalytic activity of the prepared materials was tested in a high-throughput kinetics screening setup (HTK-S) [15], and detailed catalytic testing is provided in ESI.

2.2. Catalysts characterization

The prepared Ni-based mixed oxide catalysts were characterized with various techniques, N₂-sorption, ammonia-temperature programmed desorption (NH₃-TPD), X-ray diffraction (XRD), HR-TEM and EDS, O₂-pulse chemisorption, X-ray photoelectron spectroscopy (XPS), temperature-programmed oxidation (TPO) and elemental analysis (CHNSO). More detailed procedures are elaborated in ESI.

3. Results and discussion

3.1. Catalyst characterization

3.1.1. Physisorption and chemisorption analysis

The surface area, pore size and pore volume of the mixed oxide catalysts and physisorption isotherm are shown in Table 1 and Fig. S1, respectively. Ni/TiZr catalysts showed a slightly lower specific surface area and pore volume than the corresponding Ni/NbZr catalysts, while the pore size of the former was larger than that of the latter. The physisorption isotherm of all the catalysts were of type IV with a hysteresis loop, indicating the presence of mesoporosity. The total number of acid sites was slightly higher in Ni/Ti₁Zr₄ and Ni/Nb₁Zr₄ than Ni/Ti₁Zr₁ and Ni/Nb₁Zr₁ catalysts, indicating the contribution of acid sites from ZrO₂ (Table 1 and Fig. S2).

Table 1
Physiochemical properties Ni-based mixed metal oxide catalysts.

Entry	Catalysts	d-spacing (Å) ^(a)	Lattice parameters (Å)		Specific area (m ² /g)	Pore volume (cm ³ /g)	Pore size (nm)	Acid sites (μmol/g)
			a	c				
1	Ni/ZrO ₂	2.9570	3.5829	5.2364	NA	NA	NA	NA
2	Ni/Ti ₁ Zr ₄	2.9474	3.5725	5.2158	13	0.049	15	22.18
3	Ni/Ti ₁ Zr ₁	2.9436	3.5686	5.2069	12.4	0.045	14.5	19.07
4	Ni/Nb ₁ Zr ₄	2.9531	3.5789	5.2276	18.9	0.063	13.4	38.53
5	Ni/Nb ₁ Zr ₁	2.9512	3.5746	5.2260	19.8	0.057	11.6	33.54

(a) $2d\sin\theta = n\lambda$.

3.1.2. X-ray diffraction (XRD) and HR-TEM

The monoclinic and tetragonal phase of ZrO₂ and a fraction of TiO₂-anatase or Nb₂O₅-hexagonal phase appeared in the case of Ni/Ti₁Zr₄ (Fig. 1) and Ni/Nb₁Zr₄ (Fig. S3), respectively [16–18]. A phase transformation of ZrO₂ from monoclinic to tetragonal along with an increased intensity ascribed to TiO₂-anatase and Nb₂O₅-hexagonal peaks were observed as the concentration of TiO₂ and Nb₂O₅ increased in Ni/Nb₁Zr₁ and Ni/Ti₁Zr₁ [17]. Further, a slight shift of the peak corresponding to the tetragonal plane of ZrO₂ was observed from 30.20 to 30.34 (Ni/TiZr) or 30.26 (Ni/NbZr) due to the incorporation of Ti and Nb into the ZrO₂ matrix, substantiating the formation of Ti_{1-x}Zr_xO₂ and Nb_{1-x}Zr_xO₂ solutions as in line with the changes in the lattice parameters (Table 1) [18,19].

A slight decrease in lattice parameters can be attributed to the contraction of the ZrO₂ (ionic radius of Zr⁴⁺: 0.84 Å) lattice due to incorporating an atom with a smaller ionic radius, Ti⁴⁺ (0.64 Å) or Nb⁵⁺ (0.7 Å) [19,20]. Moreover, no peak related to NiO was observed, suggesting either a high dispersion or a quantity below the detection limit. The HRTEM-EDS elemental mapping images displayed that Ni/Ti₁Zr₄ and Ni/Nb₁Zr₄ had a more uniform distribution of Ni than Ni/Ti₁Zr₁ and Ni/Nb₁Zr₁, which showed dense TiO₂ and Nb₂O₅ particles, respectively (Fig. S4 a–d). In addition, elemental mapping images of Ni/Ti₁Zr₄ and Ni/Nb₁Zr₄ show that the Ti or Nb and Zr are homogeneously distributed in the mixed oxide catalysts.

3.1.3. X-ray photoelectron spectroscopy (XPS)

Fig. S5 shows XPS spectra of Ni2p_{3/2} of mixed oxide catalysts with a major peak at 855.35 eV, which can be attributed to Ni²⁺ on the surface. However, in the case of Ni/Nb₁Zr₄, the major peak slightly shifted towards higher binding energy, which is attributed to strong metal-support interactions. A satellite peak at 861.7 eV was also observed [21]. A spin-orbit doublet peak belonging to Zr3d of ZrO₂ was observed at 181.8 and 184.2 eV, indicating that zirconium is in Zr⁴⁺ state (Fig. S6)

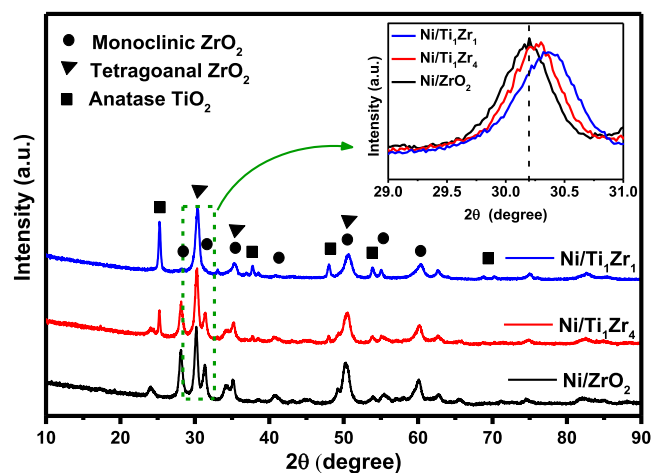


Fig. 1. XRD patterns of Ni-based TiZr mixed oxide catalysts.

[22]. Similarly, a doublet peak corresponding to Ti2p of TiO₂ and Nb3d of Nb₂O₅ was observed at 458.2 and 463.9 and 206.8 and 209.5 eV, respectively (Fig. S7) [23]. Moreover, it can be noted that the binding energy of both Ti⁴⁺ and Nb⁵⁺ slightly shifted to lower binding energy from 458.07 to 457.82 eV (Ni/Ti₁Zr₄) (Fig. S7a) and 206.74 to 206.56 eV (Ni/Nb₁Zr₄) (Fig. S7b), respectively, manifesting the transfer of an electron from ZrO₂ to Nb₂O₅ and TiO₂, resulting in the formation of Ti-O-Zr or Nb-O-Zr network as in good agreement with the XRD results [13]. The consequence of this reduction process ensured the generation of oxygen vacancy sites by partial reduction of Ti⁴⁺ and Nb⁵⁺, leading to a slight shift towards lower binding energy (458.07 to 457.82 eV) and (206.74 to 206.56 eV), respectively [13].

Fig. 2 displays the spectra of O1s peak of mixed oxide catalysts, and after deconvolution, two major peaks were observed at 529.6 and 530.7 eV, attributed to the lattice oxygen (O_α) and oxygen vacancy or adsorbed oxygen (O_β), respectively [24]. Interestingly, the oxygen vacancy concentration (O_β/O_α + O_β) was significantly higher in Ni/Ti₁Zr₄ and Ni/Nb₁Zr₄ than in Ni/Ti₁Zr₁ and Ni/Nb₁Zr₁ (Table 2), as the uncertainty on an XPS peak fitting is orders of magnitude smaller than the difference between the measured values [25]. To substantiate further, the amount of oxygen vacancy sites were confirmed in terms of OSC by oxygen pulse chemisorption analysis (Table 2). The oxygen storage capacity determined by pulse chemisorption correlates with the oxygen vacancy determined by XPS analysis as observed in the previous studies [24,26,27]. Ni/Ti₁Zr₄ and Ni/Nb₁Zr₄ possessed a significantly higher OSC than Ni/Ti₁Zr₁ and Ni/Nb₁Zr₁, respectively, indicating the enhancement of oxygen vacancies as consistent with the XPS results (Fig. 2).

3.1.4. Hydrogen-temperature programmed reduction (H₂-TPR)

Ni/Ti₁Zr₁ showed a low-intensity peak at 357 °C, corresponding to NiO (Fig. S8). This peak slightly shifted to lower temperature with a slight increment in H₂ consumption in the case of Ni/Ti₁Zr₄, indicating the increment of lower-temperature-reducible NiOx species. Likewise, a similar shift was observed in Ni/NbZr catalysts, further validating that increasing the ZrO₂ content facilitated the formation of easily reducible species. Moreover, a more pronounced peak was observed at around 585 and 700 °C for Ni/TiZr and Ni/NbZr catalysts, respectively, corresponding to NiOx strongly interacting with the support [28].

Table 2

The OSC and oxygen vacancy sites of mixed metal oxide catalysts.

Catalysts	OSC (mmol/g)	O _β /O _{α+β}
Ni/Ti ₁ Zr ₁	0.029	0.407
Ni/Ti ₁ Zr ₄	0.100	0.471
Ni/Nb ₁ Zr ₁	0.045	0.375
Ni/Nb ₁ Zr ₄	0.087	0.453

3.2. Catalytic activity

The catalytic activity of mixed metal oxide catalysts was examined through anisole HDO in the HTK-S (Fig. 3). Ni/Ti₁Zr₁ maintained its anisole conversion at around 10% with an increased selectivity to phenol from 40 to 62% and a decreased benzene selectivity from 24 to 6% during the time on stream (TOS) for 24 h (Fig. 3a). When employing Ni/Ti₁Zr₄, the anisole conversion started at roughly 30%, subsequently decreasing to 10% under identical conditions (Fig. 3b). Interestingly, the benzene selectivity started at 63% and declined to 33% as the phenol selectivity increased from 10 to 37%, indicating a higher deoxygenation ability of Ni/Ti₁Zr₄. The rationale behind the higher catalytic activity was that Ni/Ti₁Zr₄ had 3.5 times higher OSC than Ni/Ti₁Zr₁ (Table 2), suggesting Ni/Ti₁Zr₄ possessed much more oxygen vacancy sites, facilitating anisole adsorption followed by HDO on or in the vicinity of Ni sites producing benzene.

In addition, XPS results revealed that Ni/Ti₁Zr₄ possessed slightly more oxygen vacancy sites than Ni/Ti₁Zr₁ (Table 2), favouring the preferential adsorption of anisole. In general, oxygen vacancy sites of a catalyst facilitate the adsorption of oxygenates such as anisole, leading to high HDO activity, as observed in the previous studies [14,26,29]. Due to higher OSC and oxygen vacancy sites, a similar catalytic activity discrepancy was observed between Ni/Nb₁Zr₄ and Ni/Nb₁Zr₁ (Fig. S9) (Table 2). Ni/NbZr catalysts exhibited a slightly higher conversion of anisole in the first two hours than the titanium counterparts (Table S1) which was attributed to the superior oxophilic character of Nb compared to Ti [30].

A plausible reaction pathway is proposed based on the results obtained in our work, complemented by literature reported results [31,32] (Scheme 1). At the initial hours of reaction, the formation of benzene, methane and phenol was predominantly observed. No demethoxylation was observed, i.e., methanol was absent in the product stream, indicating that the reaction proceeded via demethylation (DMT) of anisole

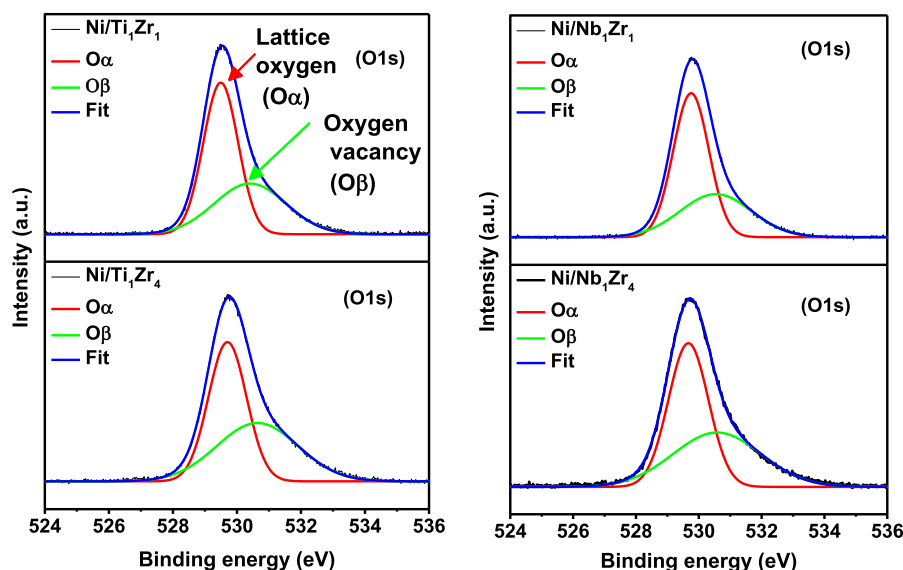


Fig. 2. The XPS spectra of O1s of Ni-based TiZr (left) and NbZr (right) mixed oxide catalysts.

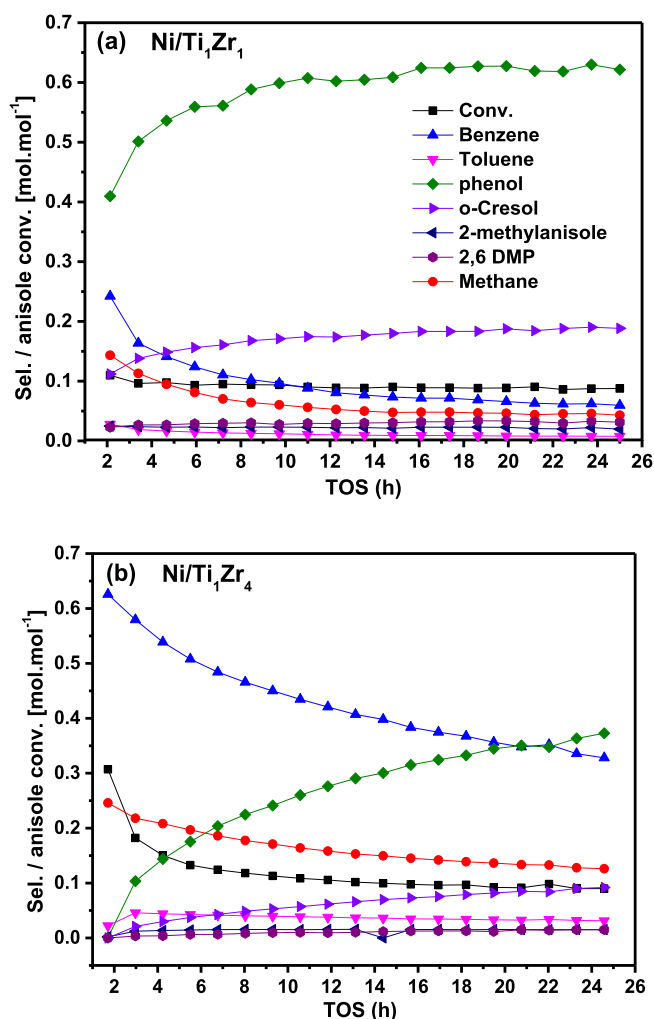
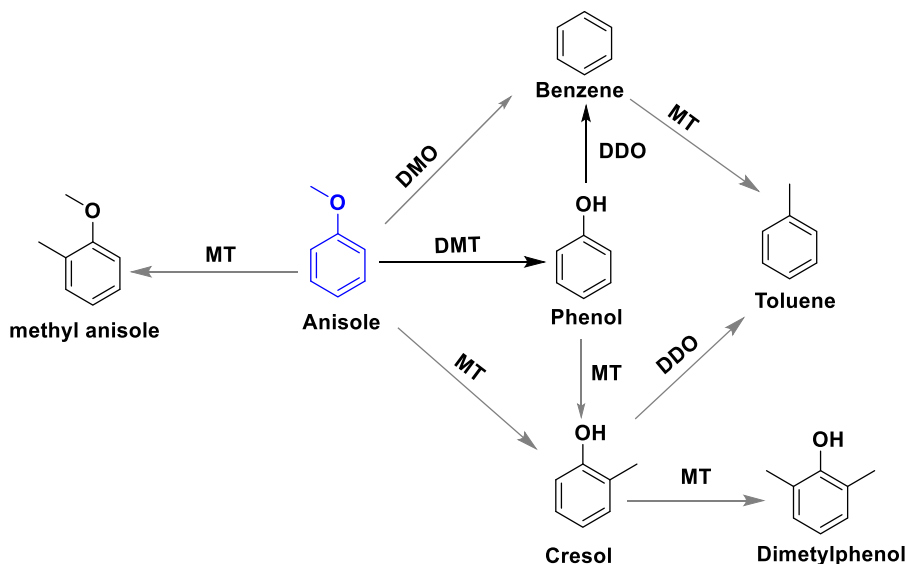


Fig. 3. Catalytic activity Ni-based mixed oxide catalysts. (Reaction conditions: $T = 340\text{ }^{\circ}\text{C}$, $P_T = 0.5\text{ MPa}$, $\text{H}_2/\text{anisole} = 50\text{ mol mol}^{-1}$, $\text{W/F}^{\circ} = 900\text{ kg}_{\text{cat}}\text{ s mol}_{\text{anisole}}^{-1}$).

to form methane and phenol. Further, benzene formation suggested the direct deoxygenation (DDO) of phenol. The demethylation of anisole over Ni together with TiZr or NbZr oxides was attributed to the preferential cleavage of $\text{C}_{\text{aliphatic}}\text{-O}$ on the Ni metal sites. This latter bond has an 84 kJ/mol lower bond dissociation energy than $\text{C}_{\text{Ar}}\text{-O}$ [31,32]. Differences in reaction chemistry on metal and oxophilic sites have been demonstrated before for anisole HDO over, Pt, Ru and Fe on SiO_2 [33]. Pt and Ru/ SiO_2 showed facile cleavage of $\text{C}_{\text{aliphatic}}\text{-O}$ (demethylation) of anisole to form phenol, followed by deoxygenation to form benzene due to the higher hydrogenation ability of Pt and Ru. Fe/ SiO_2 , on the other hand, exhibited direct deoxygenation of anisole to form benzene due to the oxophilicity character of Fe, demonstrating the reaction pathway depends on the hydrogenation ability and the oxophilicity of the metal.

Furthermore, the DDO of phenol to benzene could be promoted by the strong interaction of phenolic oxygen with the oxygen vacancy sites in Ni/Ti₁Zr₄ and Ni/Nb₁Zr₄ by reducing the energy barrier required for the C–O bond cleavage [14,26]. Interestingly, no hydrogenation products of benzene were observed, indicating the strong metal-support interaction between Ni and TiZr or NbZr, as in line with the H_2 -TPR results [10]. In addition, the limited formation of transalkylation products, such as methyl anisole, dimethyl phenol (DMP) and toluene could be attributed to Ni sites along with acidic sites (Table 1 and Fig. S2) [31,32,34]. Further, the low toluene yield could also stem from o-cresol DDO (Scheme 1). The catalytic activity of the best catalyst Ni/Nb₁Zr₄ was investigated further by increasing the space-time to 1740 $\text{kg}_{\text{cat}}\text{ s mol}_{\text{anisole}}^{-1}$; no significant changes in the product distribution were observed though the conversion increased by 20% during the first two hours, subsequently levelling off to around 30%. (Fig. S10).

The conversion of anisole over Ni/Ti₁Zr₄ and Ni/Nb₁Zr₄ catalysts steeply declined during the first 6 h TOS and remained almost unchanged afterwards, up to 24 h. Correspondingly, the benzene selectivity decreased, the phenol selectivity increased more gradually as a function of TOS. Most likely the initial sharp decline in conversion was caused by the catalyst “breaking in”, i.e. the catalyst settling in its new environment. Further deactivation was attributed to the accumulation of phenolic species over oxophilic sites and the deposition of carbon species over Ni sites [14,35]. Elemental and TPO analysis of the spent catalysts, see Fig. S11 and Table S2, corroborate that the deactivation can, indeed, be attributed to carbon deposition on all catalysts. A more thorough analysis of the spent catalyst will allow determining whether the carbon deposition on Ni sites was effectively more pronounced than



Scheme 1. The plausible reaction pathway for HDO of anisole over Ni supported on mixed oxides. MT:methyl transfer, DMT: demethylation, DMO:demethoxylation, DDO:direct deoxygenation

the phenol accumulation on the oxophilic sites. This would mean that the decreasing benzene selectivity over time occurs intrinsically and is not just the result of a conversion effect.

4. Conclusions

Enhanced the oxygen vacancy sites formation and oxygen storage capacities anisole improve the HDO activity of Ni catalysts in terms of conversion and the product distribution. Ni catalysts on Ti or Nb modified ZrO₂ supports allowed establishing this effect when the modifier was incorporated in a 1:4 ratio, i.e., Ni/X₁Zr₄ (X = Ti or Nb) catalysts were outperforming the Ni/X₁Zr₁ ones. The oxophilic sites (oxygen vacancy sites) favoured more facile adsorption of anisole compared to other, non-oxygenated, aromatic compounds, thus enhancing the selectivity towards the deoxygenated product (benzene). Moreover, the strong metal-support interaction reduces the hydrogenation capacity.

Credit author statement

HA and TV: Conceptualization, performing experiments, characterization interpretation, writing, review & editing. JL: Conceptualization, interpretation, writing, review & editing. SKK: Supervision, suggestion, review. SS: Conceptualization, interpretation, execution, supervision, funding acquisition, writing, review & editing. JWT: Conceptualization, interpretation, execution, supervision, funding acquisition, writing, review & editing.

Declaration of Competing Interest

There is no conflict of interest to declare.

Acknowledgements

This work is financially supported by the ERC consolidator grant (i-CaD) and EC (GA no 615456). The authors would like to thank the Center of Innovative and Applied Bioprocessing (CIAB), Mohali and Laboratory of Chemical Technology (LCT), Ghent University, Belgium, for unceasing financial support for providing infrastructural facilities for conducting R & D activities. HA gratefully thank the Council of Scientific & Industrial Research (CSIR), Government of India for offering Senior Research Fellowship (CSIR-SRF) and Energy Research Centre, Panjab University for PhD registration. H.A. would like to thank the ERC consolidator grant (i-CaD) and EC (GA no 615456) for financial support while working at LCT. T.V. and J.L. would like to thank the Research Foundation - Flanders (FWO) for the financial support of this project (grant numbers: 3S042419 and 12Z2218N).

Appendix A. Supplementary data

Supplementary data to this article can be found online at <https://doi.org/10.1016/j.catcom.2022.106436>.

References

- [1] G.W. Huber, S. Iborra, A. Corma, *Chem. Rev.* 106 (2006) 4044–4098.
- [2] Q. Bu, H. Lei, A.H. Zacher, L. Wang, S. Ren, J. Liang, Y. Wei, Y. Liu, J. Tang, Q. Zhang, R. Ruan, *Bioresour. Technol.* 124 (2012) 470–477.
- [3] H. Nguyen Lyckeskog, C. Mattsson, L.E. Åmand, L. Olausson, S.I. Andersson, L. Vamling, H. Theliander, *Energy Fuel* 30 (2016) 3097–3106.
- [4] V.O. Gonçalves, C. Ciotonea, S. Arrii-Clacens, N. Guignard, C. Roudaut, J. Rousseau, J.M. Clacens, S. Royer, F. Richard, *Appl. Catal. B Environ.* 214 (2017) 57–66.
- [5] J. Zhang, J. Sun, Y. Wang, *Green Chem.* 22 (2020) 1072–1098.
- [6] M.M. Ambursa, J.C. Juan, Y. Yahaya, Y.H. Taufiq-Yap, Y.C. Lin, H.V. Lee, *Renew. Sust. Energ. Rev.* 138 (2021) 110667.
- [7] C. Chen, G. Chen, F. Yang, H. Wang, J. Han, Q. Ge, X. Zhu, *Chem. Eng. Sci.* 135 (2015) 145–154.
- [8] L. Nie, P.M. de Souza, F.B. Noronha, W. An, T. Sooknoi, D.E. J. Mol. Catal. A Chem. 388 (2014) 47–55.
- [9] Y. Zheng, N. Zhao, J. Chen, *Appl. Catal. B Environ.* 250 (2019) 280–291.
- [10] Y. Yang, C. Ochoa-Hernández, A. Víctor, P. Pizarro, J.M. Coronado, D.P. Serrano Chen, *Appl. Catal. B Environ.* 145 (2014) 91–100.
- [11] L. Li, L. Dong, X. Liu, Y. Guo, Y. Wang, *Appl. Catal. B Environ.* 260 (2020), 118143.
- [12] T.N. Phan, C.H. Ko, *Catal. Today* 303 (2018) 219–226.
- [13] M. Lu, H. Du, B. Wei, J. Zhu, M. Li, Y. Shan, J. Shen, C. Song, *Ind. Eng. Chem. Res.* 56 (2017) 12070–12079.
- [14] K.A. Resende, A.H. Braga, F.B. Noronha, C.E. Hori, *Appl. Catal. B Environ.* 245 (2019) 100–113.
- [15] K.V.D. Borghat, K. Toch, V.V. Galvita, J.W. Thybaut, G.B. Marin, *Catalysts* 5 (2015) 1948–1968.
- [16] N. Salah, S.S. Habib, Z.H. Khan, F. Djouider, *Radiat. Phys. Chem.* 80 (2011) 923–928.
- [17] Y. Liu, M. Tursun, H. Yu, X. Wang, *Mol. Catal.* 464 (2019) 22–28.
- [18] W. Wang, P. Zhan, Z. Xie, Z. Li, Z. Zhang, *J. Appl. Phys.* 115 (2014), 043524.
- [19] C.A. Teles, P.M. de Souza, A.H. Braga, R.C. Rabelo-Neto, A. Teran, G. Jacobs, D. E. Resasco, F.B. Noronha, *Appl. Catal. B Environ.* 249 (2019) 292–305.
- [20] A. Khaskhoussi, L. Calabrese, J. Bouaziz, E. Proverbio, *Ceram. Int.* 43 (2017) 10392–10402.
- [21] W. Song, Y. He, S. Lai, W. Lai, X. Yi, W. Yang, X. Jiang, *Green Chem.* 22 (2020) 1662–1670.
- [22] O.A. Bulavchenko, Z.S. Vinokurov, T.N. Afonasenko, P.G. Tsyrl'Nikov, S. Tsybul'ya, A.A. Saraev, V.V. Kaichev, *Dalton Trans.* 44 (2015) 15499–15507.
- [23] J.B. Li, J. Wang, J.F. Li, Y. Li, H. Yang, H.Y. Yu, X.B. Ma, X. Yaer, L. Liu, L. Miao, *J. Mater. Chem. C* 6 (2018) 7594–7603.
- [24] Y. Wang, S. Aghamohammadi, D. Li, K. Li, R. Farrauto, *Appl. Catal. B Environ.* 244 (2019) 438–447.
- [25] R. Hesse, T. Chassé, P. Streubel, A.R. Szargan, *Surf. Interface Anal.* 36 (2004) 1373–1383.
- [26] S.M. Schimming, O.D. LaMont, M. König, A.K. Rogers, A.D. D'Amico, M.M. Yung, C. Sievers, *ChemSusChem* 8 (2015) 2073–2083.
- [27] C.M. Pichler, D. Gu, H. Joshi, F. Schüth, *J. Catal.* 365 (2018) 367–375.
- [28] X. Zhang, J. Long, W. Kong, Q. Zhang, L. Chen, T. Wang, L. Ma, Y. Li, *Energy Fuel* 28 (2014) 2562–2570.
- [29] S. Jiang, N. Ji, X. Diao, H. Li, Y. Rong, Y. Lei, Z. Yu, *ChemSusChem* 14 (2021) 4377–4396.
- [30] C.A. Teles, P.M. de Souza, R.C. Rabelo-Neto, A. Teran, G. Jacobs, D.E. Resasco, F. B. Noronha, *ACS Sustain. Chem. Eng.* 9 (2021) 12870–12884.
- [31] S. Pichaikaran, P. Arumugam, *Green Chem.* 18 (2016) 2888–2899. *Appl. Catal. B: Environ.*, 208 (2017), pp. 60–74.
- [32] C. Ranga, R. Lødeng, V.I. Alexiadis, T. Rajkhowa, H. Björkan, S. Chytil, I. H. Svenum, J. Walmsley, C. Detavernier, H. Poelman, P.V.D. Voort, J.W. Thybaut, *Chem. Eng. J.* 335 (2018) 120–132.
- [33] Q. Tan, G. Wang, A. Long, A. Dinse, C. Buda, J. Shabaker, D.E. Resasco, *J. Catal.* 347 (2017) 102–115.
- [34] H. Wang, M. Feng, B. Yang, *Green Chem.* 19 (2017) 1668–1673.
- [35] P.M. de Souza, R.C. Rabelo-Neto, L.E. Borges, G. Jacobs, B.H. Davis, D.E. Resasco, F.B. Noronha, *ACS Catal.* 7 (2017) 2058–2073.